


# Computing photoelectron spectra employing unique continuum functions

Tobias Marx 

*Institut für Physik, Universität Rostock, Albert-Einstein-Strasse 23-24, 18059 Rostock, Germany*

Sergey I. Bokarev \*

*Chemistry Department, Technical University of Munich, Lichtenbergstrasse 4, Garching 85748, Germany  
and Institut für Physik, Universität Rostock, Albert-Einstein-Strasse 23-24, 18059 Rostock, Germany*



(Received 11 July 2022; accepted 26 August 2022; published 15 September 2022)

Molecular photoelectron spectra are commonly obtained theoretically in Fermi's Golden Rule framework, where the stationary continuum wave function is represented by slowly converging series such as the celebrated partial wave expansion. In this paper, we employ an alternative approach to address the photoionization cross section. While it gives the same cross section as the Golden Rule, this method follows a different route and has a number of advantages. The cross section is computed directly from the probability current density having the (conjugated) Dyson orbital as its source. With this, one arrives at an intuitive interpretation of the photoionization process and avoids employing a long expansion series since the continuum solution is transition-specific and thus unique. We expect this methodology to be particularly beneficial in the case of complexly shaped and delocalized Dyson orbitals.

DOI: [10.1103/PhysRevA.106.032806](https://doi.org/10.1103/PhysRevA.106.032806)

## I. INTRODUCTION

Photoelectron spectroscopy deserves the right to be named one of the most powerful and popular tools in physics, chemistry, and material science [1,2]. During the decades after its experimental establishment, many theoretical methods were suggested, ranging from the simplistic Koopmans' theorem to the involved multichannel scattering formalism [3–11]. Most of the weak-field approaches follow the first-order perturbative description, calculating the ionization cross sections based on Fermi's Golden Rule (FGR)

$$\sigma \propto \sum_F \left| \langle \Psi_F^N(k) | \hat{H}_{\text{int}} | \Psi_I^N \rangle \right|^2 \delta(\tilde{\omega} - E_F + E_I) \quad (1)$$

for the transition between the  $N$ -electron initial bound  $|\Psi_I^N\rangle$  and final continuum  $|\Psi_F^N(k)\rangle$  states with energies  $E_I$  and  $E_F$ .  $\hat{H}_{\text{int}}$  is the interaction Hamiltonian,  $\tilde{\omega}$  is the incoming photon energy, and  $k = |\mathbf{k}|$  is the photoelectron momentum. Note that atomic units are used throughout the article. Although Eq. (1) looks simple, the construction of the proper continuum final states is sophisticated [10,11] since one needs to consider infinitely many reference states sharing the same value of  $k$  [12]. For instance, the continuum wave function is commonly expanded in terms of a large number of partial waves [6,7,13] and their radial dependencies are attained by solving a large system of radial Schrödinger equations. However, the cross section often slowly converges with respect to the maximum angular momentum.

In contrast, in this article, we develop a frequency-domain method refraining from the use of FGR. Employing a

driven-type Schrödinger equation (SE) [14,15], the photoionization cross sections can be computed using a physically intuitive picture where an electron is transferred from its initial state [Dyson orbital (DO)] to an outgoing continuum wave that reaches the detector [16]. Thus, the conceptual way of calculating the continuum wave function and cross section differs from the most widely used approaches, suggesting several advantages. In particular, our approach produces a single wave function for a given  $k$  value where all the transition-specific information is encoded, as opposed to FGR. Therefore, this method can be especially beneficial when the Dyson orbital or molecular (scattering) potential has a complex angular structure or is delocalized, which would otherwise require long expansions of the photoelectron function.

## II. THEORY

The proposed formalism is based on the first-order perturbation theory [17] and involves concepts regarded in other [16,18,19] and similar [14,15] contexts. To set the stage, let us consider a light pulse impinging a molecule and leading to the expelling of an electron, which is measured by a detector at a considerable distance from the target (see Fig. 1). We assume an  $\boldsymbol{\varepsilon}$ -polarized unimodal electromagnetic field with the vector potential  $\mathbf{A}(\mathbf{r}, t) = A\boldsymbol{\varepsilon}e^{i\mathbf{k}\cdot\mathbf{r}-i\tilde{\omega}t} + \text{c.c.}$  and employ the time-dependent perturbation theory. Unlike FGR, we will directly concern ourselves with the probability current density of the photoelectron at the detector.

For an  $N$ -electron system with the wave function  $\Psi(\bar{\mathbf{r}}, t)$ , the current density reads (neglecting magnetic interactions)

$$\mathbf{j}(\bar{\mathbf{r}}, t) = \sum_u^N [\text{Im}\{\Psi^*(\bar{\mathbf{r}}, t)\nabla_u\Psi(\bar{\mathbf{r}}, t)\} + \hat{\mathbf{A}}(\mathbf{r}_u, t)|\Psi(\bar{\mathbf{r}}, t)|^2],$$

\*sergey.bokarev@uni-rostock.de

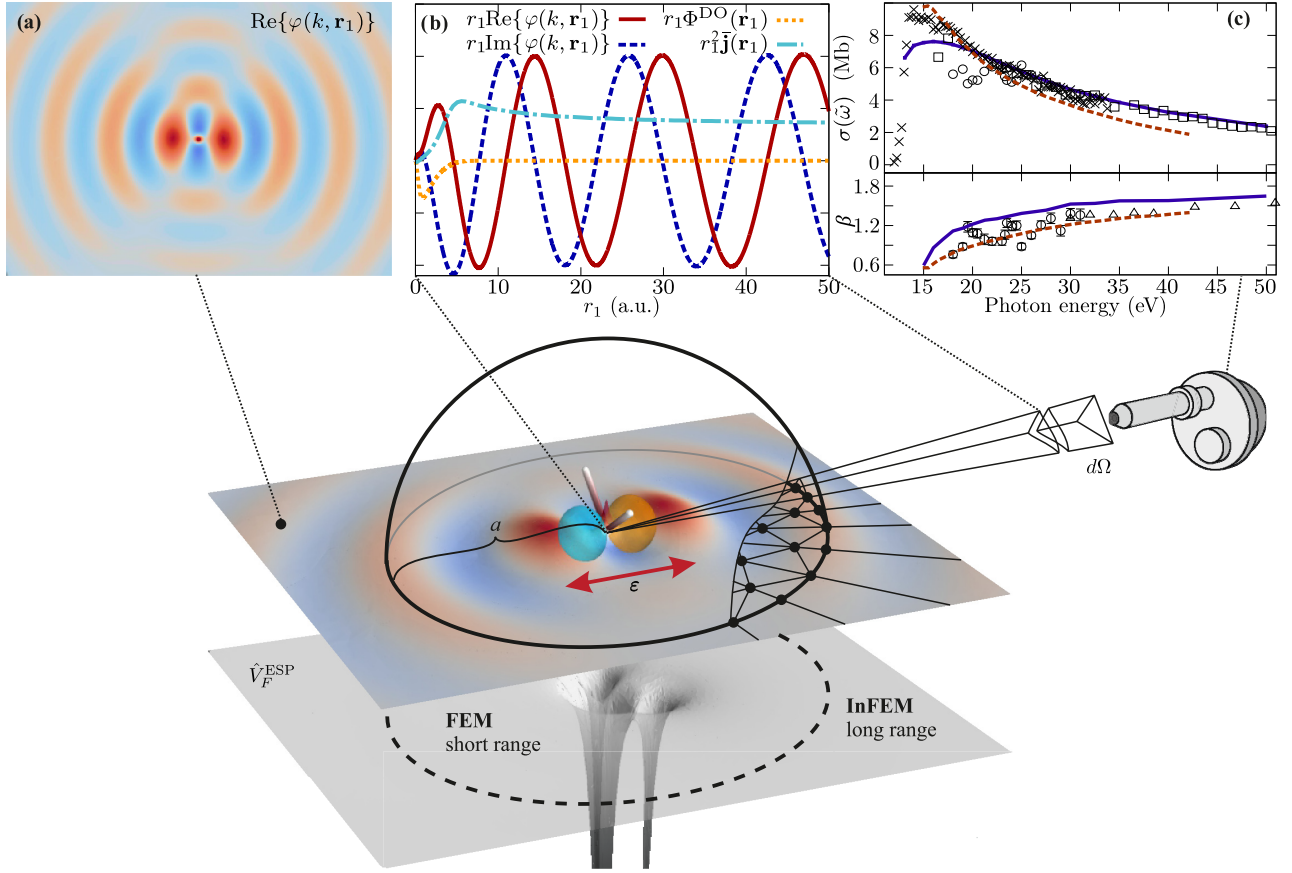


FIG. 1. A pictorial view of the method, Eq. (6), to obtain the continuum electron function  $\varphi(k, \mathbf{r}_1)$  as implemented within an (in)finite element (finite element method (FEM) augmented with infinite elements (InFEM)) framework. It is demonstrated on the example of the  $\text{H}_2\text{O}$  molecule. The lower part displays the electrostatic potential  $V_F^{\text{ESP}}(\mathbf{r}_1)$  in the molecular plane (gray surface), the molecule with its Dyson orbital ( $1b_1$ ) in the center, the sphere surrounding FEM domain (with grid points), infinite elements (half rays), and the photoelectron function  $\varphi(k, \mathbf{r}_1)$ . (a) The 2D cut of the real part of  $\varphi(k, \mathbf{r}_1)$  in the plane spanned by one of the O–H bonds and the polarization vector  $\boldsymbol{\varepsilon}$ . (b) The radial part of the Dyson orbital,  $r_1 \Phi^{\text{DO}}$ , serving as a source term, the real and imaginary parts of  $r_1 \varphi(k, \mathbf{r}_1)$ , and the probability current  $r_1^2 \bar{\mathbf{j}} \cdot \mathbf{n}_{r_1}$ , see Eq. (10), along the polarization axis. (c) the computed  $1b_1$ -ionization cross section of water  $\sigma(\tilde{\omega})$  and asymmetry parameter  $\beta$  (solid blue curves) as compared to experimental data (crosses ( $\times$ ) [20], squares ( $\square$ ) [21], circles ( $\circ$ ) [22], and triangles ( $\triangle$ ) [23]). Shown are also the theoretical results digitized from Moitra *et al.* [24] (dashed red curves).

where  $\bar{\mathbf{r}} = (\mathbf{r}_1, \dots, \mathbf{r}_N)$ . It naturally partitions according to the orders of perturbation theory if one inserts the expansion  $\Psi(\bar{\mathbf{r}}, t) = \Psi^{(0)}(\bar{\mathbf{r}}, t) + \Psi^{(1)}(\bar{\mathbf{r}}, t) + \dots$ . Since  $\Psi^{(0)}(\bar{\mathbf{r}}, t)$  is the initial bound state's wave function  $\Psi_I^{(0)}$ , it vanishes exponentially at  $r_u \rightarrow \infty$  ( $u = 1, \dots, N$ ) [25]. On the contrary, the final wave function  $\Psi_F^N(\bar{\mathbf{r}}, t)$  does not vanish at the detector ( $r_1 \rightarrow \infty$ ) if it contains a continuum orbital  $\varphi(k, \mathbf{r}_1)$ . (Here, we implied without loss of generality that the continuum electron corresponds to  $\mathbf{r}_1$ .) Analyzing the perturbative contributions to the current, one sees that all terms apart from  $\Psi^{(1)*}(\bar{\mathbf{r}}, t) \nabla \Psi^{(1)}(\bar{\mathbf{r}}, t)$  vanish at  $r_1 \rightarrow \infty$  when other electrons  $2, \dots, N$  stay confined close to their distribution in the initial bound state  $\Psi_I^{(0)}$ . Therefore, up to the second order in perturbation theory, the probability current density at the detector is dictated by the first-order correction to the wave function

$$\mathbf{j}(\bar{\mathbf{r}}, t) \xrightarrow[r_{u \neq 1} < \infty]{r_1 \rightarrow \infty} \sum_u^N \text{Im}\{\Psi^{(1)*}(\bar{\mathbf{r}}, t) \nabla_u \Psi^{(1)}(\bar{\mathbf{r}}, t)\}. \quad (2)$$

This wave function obeys the well-known equation from the time-dependent perturbation theory

$$(\hat{H}^{(0)}(\bar{\mathbf{r}}) - \omega) \Psi^{(1)}(\bar{\mathbf{r}}) = -iAe^{i\mathbf{k}\mathbf{r}} \boldsymbol{\varepsilon} \cdot \sum_u^N \nabla_u \Psi^{(0)}(\bar{\mathbf{r}}) \quad (3)$$

with  $\omega = E_I^{(0)} + \tilde{\omega}$  and satisfies Sommerfeld's radiative boundary condition [26]

$$r_1 \left( \frac{\partial}{\partial r_1} - ik \right) \Psi^{(1)}(\bar{\mathbf{r}}) \xrightarrow[r_1 \rightarrow \infty]{} 0. \quad (4)$$

Next, we assume  $\Psi^{(1)}(\bar{\mathbf{r}})$  to have the form of the antisymmetrized product of the ionic bound state  $\Psi_F^{N-1}$  and the continuum electron orbital  $\varphi(k, \mathbf{r}_1)$

$$\Psi^{(1)}(\bar{\mathbf{r}}) = \mathcal{A}\{\varphi(k, \mathbf{r}_1) \Psi_F^{N-1}(\mathbf{r}_2, \dots, \mathbf{r}_N)\}. \quad (5)$$

Thus, we limit ourselves with the single-channel scattering, neglect autoionization, and assume the sharp value of the

photoelectron's momentum  $k$ ; these limitations can be lifted leading to a more complicated formalism.

Further, we make use of the well-established Dyson orbital concept [4]. Inserting expression (5) in Eq. (3), multiplying it with  $\Psi_F^{N-1,\dagger}(\mathbf{r}_2, \dots, \mathbf{r}_N)$ , and integrating over the bound electron coordinates  $\mathbf{r}_2, \dots, \mathbf{r}_N$ , one obtains the following working equation for  $\varphi(k, \mathbf{r}_1)$  in the velocity gauge:

$$\begin{aligned} & \left( \hat{T} + \hat{V}_F^{\text{ESP}} + \hat{V}_X + \hat{W} - \frac{k^2}{2} \right) \varphi(k, \mathbf{r}_1) \\ & = -iA\boldsymbol{\varepsilon} \cdot (\nabla \Phi_{IF}^{\text{DO}} + \tilde{\Phi}_{IF}^{\text{DO}}). \end{aligned} \quad (6)$$

This equation represents an inhomogeneous (driven) variant of the usual SE  $(\hat{T} + \hat{V}_F^{\text{ESP}} + \hat{V}_X + \hat{W} - k^2/2)\varphi(k, \mathbf{r}_1) = 0$  for the motion of an electron with the total energy  $k^2/2$  in the effective mean-field electrostatic potential (ESP) of the final state  $\hat{V}_F^{\text{ESP}}$ ; the later equation is commonly considered to determine continuum orbitals. The nonlocal operators  $\hat{V}_X$  and  $\hat{W}$  account for the interaction of the photoelectron with the bound electrons of the ion beyond the action of mean-field potential  $\hat{V}_F^{\text{ESP}}$ , i.e., they correspond to the exchange and correlation. However, Eq. (6) has an essential difference from the homogeneous SE due to the presence of inhomogeneous terms. These terms include the gradient of the DO and the conjugate DO,  $\tilde{\Phi}_{IF}^{\text{DO}}$ , which can be expressed in terms of initial state orbitals  $\{\phi_j\}$

$$\begin{aligned} \Phi_{IF}^{\text{DO}} &= \sum_q \langle \Psi_F^{N-1} | \hat{a}_q | \Psi_I^N \rangle \phi_q, \\ \tilde{\Phi}_{IF}^{\text{DO}} &= \sum_{pq} \langle \Psi_F^{N-1} | \hat{a}_p^\dagger \hat{a}_q \hat{a}_s | \Psi_I^N \rangle \langle \phi_p | \nabla | \phi_q \rangle \phi_s. \end{aligned} \quad (7)$$

The inhomogeneity serves as a source of probability current due to the dipole transition from the DO to  $\varphi(k, \mathbf{r}_1)$ , and dictates the shape of the later, Fig. 1(b). Here, the boundary condition, Eq. (4), enforces the proper relation between the real and imaginary parts of  $\varphi(k, \mathbf{r}_1)$ . All results shown in the present work are obtained with the length-gauge expression and omitting the operators  $V_X$  and  $\hat{W}$

$$\left( \hat{T} + \hat{V}_F^{\text{ESP}} - \frac{k^2}{2} \right) \varphi(k, \mathbf{r}_1) = i\tilde{\omega}A\boldsymbol{\varepsilon} \cdot (\hat{\mathbf{r}}_1 \Phi_{IF}^{\text{DO}} + \tilde{\Phi}_{IF}^{\text{DO},r}). \quad (8)$$

Thus our results correspond to the usual level of DO theory when including the conjugate DO.

The  $\varphi(k, \mathbf{r}_1)$  obtained from Eq. (6) can be used to calculate the photoelectron probability current far from the molecule, while the other electrons stay unobserved. Thus, we compute the reduced current

$$\bar{\mathbf{j}}(\mathbf{r}_1) = \int d\mathbf{r}_2 \dots d\mathbf{r}_N \mathbf{j}(\bar{\mathbf{r}}) \xrightarrow{r_1 \rightarrow \infty} \text{Im}\{\varphi^*(k, \mathbf{r}_1) \nabla \varphi(k, \mathbf{r}_1)\}, \quad (9)$$

which is used to estimate the differential cross section as

$$\frac{d\sigma}{d\Omega} = \lim_{r_1 \rightarrow \infty} 2\pi \frac{r_1^2 \mathbf{n}_{r_1} \cdot \bar{\mathbf{j}}(\mathbf{r}_1)}{c\tilde{\omega}A^2} \quad (10)$$

with the radial unit vector  $\mathbf{n}_{r_1}$ .

### III. NUMERICAL PROCEDURE

The implementation used in this work utilizes space partitioning to solve the unbounded photoelectron wave problem, Eq. (8), with boundary conditions Eq. (4). The inner region has an approximately ellipsoidal shape and encompasses the domain where the highly molecule-specific source terms and the short-range potential are nonvanishing. In this region, the photoelectron is represented by second-order tetrahedral finite elements (FEM), see Fig. 1. The outer region accounts for the long-range Coulomb potential and implements the outgoing boundary conditions using infinite elements (InFEM) [27,28]. The InFEM represents a layer of elements that extend from the outer surface of the FEM region in the radial direction up to infinity. Thereby, one makes use of the known asymptotic behavior of the solution [29] by using element-wise basis (trial) functions of the form

$$\chi_i(\mathbf{r}) = \chi_b(\mathbf{r}_\perp) P_n^{(2,0)}\left(\frac{1}{r}\right) \frac{\exp\{ikr + i\frac{Z}{k} \ln r\}}{r}, \quad (11)$$

where  $\chi_b(\mathbf{r}_\perp)$  is a polynomial in two ‘‘angular’’ directions,  $P_n^{(2,0)}(x)$  is a radial Jacobi polynomial of order  $n$  [30], and  $Z$  is the net charge of the ionized system. These basis functions naturally incorporate the outgoing boundary conditions and thus represent a very powerful technique to address outgoing wave problems.

Our implementation makes intensive use of the LIBMESH numerical library [31] and utilizes infinite elements of the Astley-Leis form [32,33], which are modified to account for the Coulombic tail of the potential. While finite elements in the FEM region provide a versatile basis due to their low order, they are not efficient for accurately describing highly oscillating functions. To reduce the computational effort, we multiply the FEM basis with an oscillatory function depending on the ‘‘local’’ kinetic energy, see the Appendix. The FEM mesh used for the calculation is constructed as a Delaunay tetrahedralization using the TETGEN library [34]. The generating set of points forms ellipsoidal layers around the atoms, cutting off the overlapping atomic regions. The distance between points is estimated according to the spatial gradient of the bound-state orbitals and kinetic energy. After solving the eigensystem, we refine the mesh adaptively, using Kelly's error estimate [35].

The initial and ionic bound states are computed with GAUSSIAN 16 [36], using the aug-cc-pV5Z basis [37–40] with the optimally tuned LC-BLYP functional. The functional is adjusted in a nonempirical way to better reproduce photoionization-related quantities according to the protocol described in Ref. [41]. The obtained range-separation parameters are  $\alpha = 0.0$ ,  $\omega = 0.59$  (a.u.)<sup>-1</sup> for argon and  $\alpha = 0.05$ ,  $\omega = 0.50$  (a.u.)<sup>-1</sup> for the H<sub>2</sub>O molecule. The  $(3s)^{-1}$  excited state of the Ar<sup>+</sup> ion and the  $(1b_2)^{-1}$  and  $(3a_1)^{-1}$  states of the H<sub>2</sub>O<sup>+</sup> ion are calculated with Tamm-Dancoff approximation to time-dependent DFT. The electrostatic potential  $\hat{V}_F^{\text{ESP}}$  is obtained by solving the Poisson equation with FEM.

### IV. RESULTS

Neglecting for simplicity the  $V_X$  and  $\hat{W}$  terms, i.e., using Eq. (8), the formalism is applied to two prototypical systems:

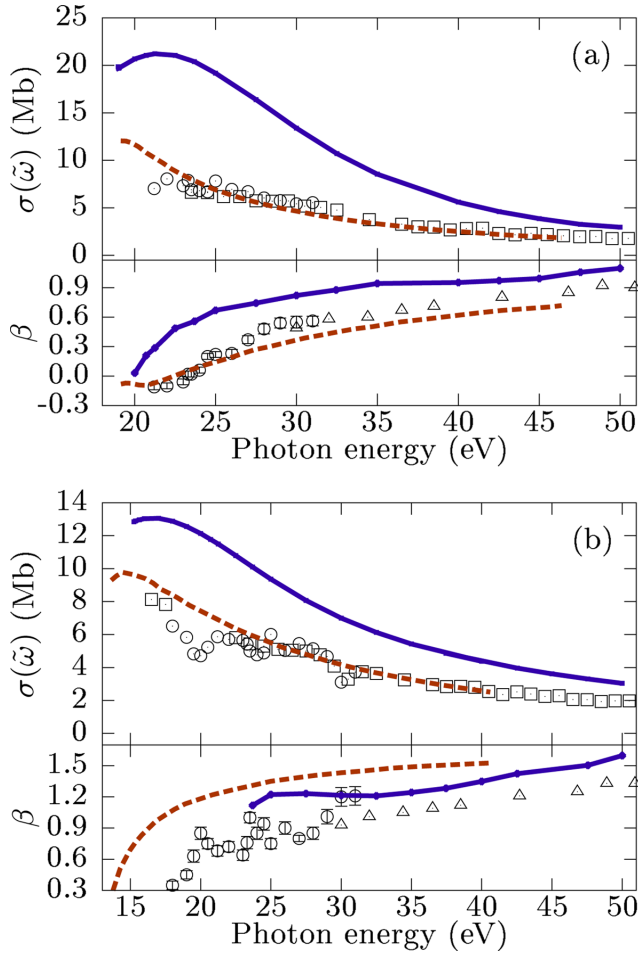


FIG. 2. Computed cross sections and asymmetry parameters (blue solid lines) for the (a)  $1b_2$  and (b)  $3a_1$  ionization of the water molecule. Experimental data: squares ( $\square$ ) [21]; circles ( $\circ$ ) [22]; triangles ( $\Delta$ ) [23]. Dashed red lines: Theoretical results digitized from Moitra *et al.*, Ref. [24], see text for details.

the  $3s$  and  $3p$  ionization of atomic argon and the  $1b_1$ ,  $1b_2$ , and  $3a_1$  ionization of the water molecule.

The cross section of water  $1b_1$  ionization is given in Fig. 1(c). Overall, our result reproduces the form of the experimental cross section and is in good agreement for photon energies above 20 eV (kinetic energy  $>7$  eV). The cross section in the region of the maximum at about 15 eV is underestimated by 10%. Note, however, that the experimental data are not always in accord with each other, especially in the low kinetic energy region. The asymmetry  $\beta$ -parameter displayed in the lower tier of Fig. 1(c) is also well reproduced. In addition to our results, the calculations of Moitra *et al.* [24] are shown for comparison. These data are also obtained with density functional theory (DFT), but treating all electrons on the same footing, i.e., exchange and correlation between the photoelectron and bound orbitals are included at the DFT level.

The cross sections and  $\beta$  parameters for the other two transitions of water are shown in Fig. 2. Although at low kinetic energies the cross sections are notably overestimated by a factor of 3 for the  $1b_2$  ionization [Fig. 2(a)] and by a factor

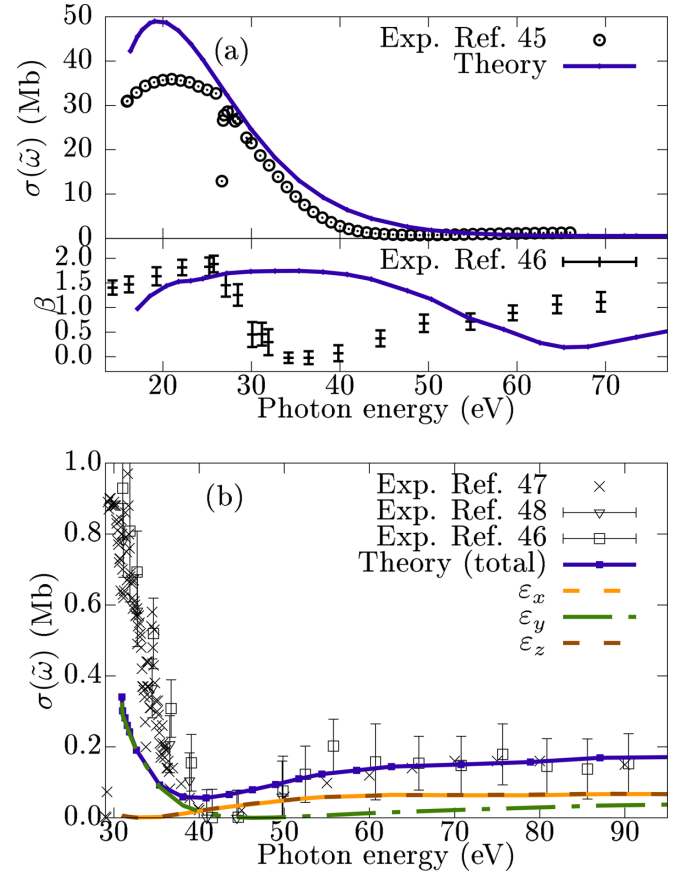


FIG. 3. Computed cross section for the argon (a)  $3p$  and (b)  $3s$  ionization as compared to experimental data. In panel (b), the total spherically averaged theoretical cross section (blue solid curve) is decomposed in its polarization components ( $\varepsilon_y$  dash-dotted green line and coinciding  $\varepsilon_x$  and  $\varepsilon_z$  dashed orange and red lines). Experimental data from Refs. [45–48].

of 2 for the  $3a_1$  [Fig. 2(b)], they converge to the experimental values for larger kinetic or photon energies. The  $\beta$  parameters in both cases reasonably reproduce the experiment.

The discrepancies observed for the cross sections at maxima can be connected to the implicit inclusion of only some of the intrachannel couplings via the DFT treatment and neglect of the bound-continuum exchange and interchannel couplings [42]. Similar behavior can still be observed when correlation effects are treated on the higher level [24] (dashed red curves), but at lower kinetic energies. In the case of  $1b_1$  ionization, one considers a neutral-ground-state to ionized-ground-state transition and can expect better reproducibility of the experiment as both states result from the self-consistent DFT treatment. In contrast,  $(1b_2)^{-1}$  and  $(3a_1)^{-1}$  final states are treated with the linear-response Tamm-Dancoff method and may lack important intrachannel interactions. The later consideration and neglect of  $\hat{W}$  and  $\hat{V}_X$  terms in Eq. (8) explain larger deviations at low kinetic energies for these two transitions.

The data for the  $3p$  ionization of the Ar atom are displayed in Fig. 3(a). The results demonstrate similar trends to those discussed for water, with the cross section at low kinetic energies being overestimated. The effects causing the dips due to Rydberg resonances and the Cooper minimum, barely visible

at about 47 eV in the experiment, are not included in our model due to the ansatz of Eq. (5). Note that the dependence of the  $\beta$  parameter on photon energy is not well reproduced. To get this dependence correctly would require the inclusion of exchange effects [24].

The results for argon 3s ionization are shown in Fig. 3(b) and agree reasonably well with the experimental data. They display a Cooper minimum which occurs at slightly lower photon energies than in the experiment, but more importantly, the cross section at minimum is nonzero. This deficiency can be attributed to the broken-symmetry character of the ionic ground-state Kohn-Sham solution due to orbital relaxation, making different 3p orbitals of argon nondegenerate. This leads to different contributions of the conjugate DO Cartesian components [dashed and dash-dotted curves in Fig. 3(b)] to the cross section. Thus, the total result represents the average of the qualitatively correct behavior for the y polarization of the incoming photon, having a minimum around 47 eV and spurious x and z components with the minimum at 35 eV and no rise of the cross section for small kinetic energies. Finally, we note that the presence and position of the Cooper minimum in the Ar 3s ionization cross section poses a challenge for theory [43]. Depending on the applied methodology, different authors ascribed it to the influence of intrachannel [24], interchannel [42], or exchange [44] interactions.

## V. DISCUSSION

The suggested method represents a reformulation of the FGR approach and it can be shown that both theories produce identical cross sections [12,49]. Nevertheless, the working equations and boundary conditions are different. While for FGR, the homogeneous SE and scattering boundaries [10,11] are used, in our approach, the inhomogeneous (driven-type) SE with the outgoing boundary of Eq. (4) is employed. Thus, the continuum wave functions in both approaches have different properties and should be interpreted differently. For instance, the well-known optical theorem [12] loses its sense for our formulation as we have no ingoing electron wave and, thus, no forward scattering direction.

As illustrated in Fig. 4, both theories use the same ingredients but vary in the recipes to obtain the cross section. In the FGR [Fig. 4(a)], one solely uses final-state-specific terms ( $\hat{V}_F^{\text{ESP}}$ , correlation, and exchange) to obtain a large number of continuum functions  $\psi_{lm}(k, \mathbf{r}_1)$ . Since they do not contain information on the initial state  $|\Psi_I^N\rangle$  and the details of light-matter interaction ( $\hat{H}_{\text{int}}$ ), they are unspecific to the particular transition triggered by a particular pulse. These solutions *en masse* could be suitable for various individual ionization channels  $I \rightarrow F, l, m$  which often lie outside our interest. Only at the stage of taking the overlap,  $\langle \Phi_{IF}^{\text{DO}} | \hat{H}_{\text{int}} | \psi_{lm}(k, \mathbf{r}_1) \rangle$ , Fig. 4(a), their contributions to the cross section are sorted out according to their relevance.

In contrast, in our approach, the equation determining  $\varphi(k, \mathbf{r}_1)$  contains both  $\hat{V}_F^{\text{ESP}}$  as well as transition-specific information entering via inhomogeneous terms, see Eq. (6). Therefore, one avoids the need for possibly slowly converging expansions. Instead,  $\varphi(k, \mathbf{r}_1)$  is uniquely determined both in its shape and normalization by the set of  $I, F, k$ , and the

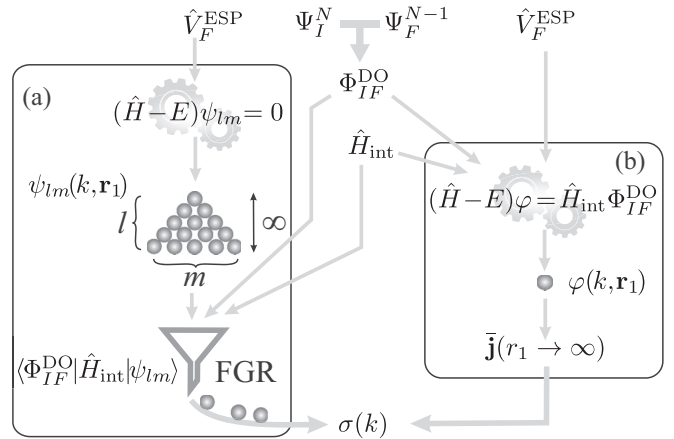


FIG. 4. Schematic illustrating the relation between (b) the developed approach to the standard procedure based on (a) the FGR and the respective pathways to obtain the cross section.

form of  $\hat{H}_{\text{int}}$ . Thus, one obtains a unique solution for a given  $k$  which, in terms of the partial wave expansion, inherently incorporates the proper combination of the contributions with different  $l$  and  $m$ . For instance, in water  $1b_1$  ionization, the wave function computed for  $k^2/2 = 37.2$  eV and a polarization normal to the molecular plane, which is shown in Fig. 1(a), represents the superposition of  $s$  and  $d$  waves distorted by the molecular potential.

To understand the present framework, one recalls that the DO has a physical sense of the photoelectron’s quasiparticle wave function “before” ionization. In the proposed formalism, it plays the role of a source for the outgoing electron wave which reaches the detector at  $\mathbf{r}_1 \rightarrow \infty$ . Thus, the suggested method provides a more intuitive interpretation of the photoionization process than FGR, which formulates the cross section in the form of an overlap, Eq. (1).

To comply with the proposed picture of an outgoing wave one needs to ensure a proper boundary condition. In that sense, infinite elements are vital for the practical implementation as they not only incorporate outgoing boundary, Eq. (4), but allow for easy evaluation of the probability current at  $\mathbf{r}_1 \rightarrow \infty$ : in the infinite-element ansatz, Eq. (11), the only contribution to  $\vec{\mathbf{j}}(\mathbf{r}_1)$  surviving at  $r_1 \rightarrow \infty$  is due to the lowest-order (constant) term of  $P_n(1/r)$ . Several alternative techniques implementing the outgoing boundary conditions are available, e.g., complex absorbing potentials [50]. However, they require the diligent choice of parameters, with the proposed formalism being free from such need. Moreover, evaluating the asymptotic photocurrent requires large simulation boxes when applied together with absorbing boundaries.

Finally, we note that the partial-wave expansion is a technical aspect of solving the SE and can also be employed for its driven inhomogeneous variant [15,19,51]. In such a scheme, one requires to solve possibly many radial [one-dimensional (1D)] equations that are nontrivially coupled due to the non-spherical potential [7]. As we show here, one can succeed without such expansion, solving the three-dimensional (3D) equation as a whole. Due to the involvement of infinite elements and augmenting with oscillator functions (see the Appendix), one can select the finite element region to be small

and coarse, keeping, despite inherently cubic growth with the simulation box size, the computational demand relatively modest.

## VI. CONCLUSION

To conclude, this article suggests an alternative perspective on the theoretical approach to photoelectron spectra. It is based on the well-known expressions from the first-order time-dependent perturbation theory formulated in the form of driven SE. The generic  $N$ -electron problem is reduced to an effective one-electron equation using the Dyson orbital concept. The presented approach provides a natural interpretation of the photoionization process regarding the source and outflow of the electron's wave. Notably, we do not employ Fermi's Golden Rule and compute the photocurrent directly. Further, the formalism provides a unique photoelectron function and does not involve partial-wave expansion. Note, however, that the present methodology is applicable only when monochromatic light is involved, thus, leaving aside ionization by ultrashort pulses (the situation which would require an explicit time-domain treatment).

For illustration, formalism is applied to the computation of cross sections and asymmetry parameters for the valence ionization of the argon atom and water molecule. However, we foresee this approach be beneficial for systems with very delocalized or complexly shaped DOs, e.g., in 1D or two-dimensional (2D) systems or for molecules adsorbed and substantially altered by surfaces or affected by the near-field effects. These perspectives will require further development of the formalism.

## ACKNOWLEDGMENTS

Financial support from the Deutsche Forschungsgemeinschaft Grant No. BO 4915/1-1 and Landesgraduiertenförderung of Mecklenburg-Vorpommern is gratefully acknowledged.

## APPENDIX: OSCILLATOR FUNCTION

The oscillator function in the FEM region recovers the oscillation of the photoelectron function allowing for finite element sizes exceeding the wavelength. It is unity  $O(|\mathbf{r} - \mathbf{r}_0|) = 1$  if  $|\mathbf{r} - \mathbf{r}_0| < a_0$ , i.e., in the inner region where the photoelectron wave experiences substantial interference due to contributions from different atoms. In the outer region  $|\mathbf{r} - \mathbf{r}_0| > a_1$ , it oscillates according to the local momentum  $p_{\text{loc}} = \sqrt{2(E_{\text{tot}} + V_F^{\text{ESP}}(\mathbf{r}))}$

$$O(|\mathbf{r} - \mathbf{r}_0|) = \exp[ip_{\text{loc}}|\mathbf{r} - \mathbf{r}_0|]. \quad (\text{A1})$$

In the region  $a_0 < |\mathbf{r} - \mathbf{r}_0| < a_1$ , the smooth transition is ensured by the function  $s(x) = (6x^2 - 15x + 10)x^3$

$$O(|\mathbf{r} - \mathbf{r}_0|) = \exp\left[is\left(\frac{|\mathbf{r} - \mathbf{r}_0|}{a_1 - a_0}\right)p_{\text{loc}}|\mathbf{r} - \mathbf{r}_0|\right]. \quad (\text{A2})$$

Here  $\mathbf{r}_0$  is the origin; parameters  $a_0$  and  $a_1$  are selected to encompass the molecular region and ensure a smooth transition to the outer region. For molecular systems, ellipsoidal shapes of the regions are used, making  $a_0$  and  $a_1$  angular-dependent.

- 
- [1] *Very High Resolution Photoelectron Spectroscopy*, Lecture Notes in Physics No. 715, edited by S. Hüfner (Springer, Berlin, 2007).
- [2] S. Suga, A. Sekiyama, and C. Tusche, *Photoelectron Spectroscopy: Bulk and Surface Electronic Structures*, Springer Series in Surface Sciences, Vol. 72 (Springer International Publishing, Cham, Germany, 2021).
- [3] D. P. Chong, O. V. Gritsenko, and E. J. Baerends, Interpretation of the Kohn–Sham orbital energies as approximate vertical ionization potentials, *J. Chem. Phys.* **116**, 1760 (2002).
- [4] B. T. Pickup, On the theory of fast photoionization processes, *Chem. Phys.* **19**, 193 (1977).
- [5] P. W. Langhoff, C. T. Corcoran, J. S. Sims, F. Weinhold, and R. M. Glover, Moment-theory investigations of photoabsorption and dispersion profiles in atoms and ions, *Phys. Rev. A* **14**, 1042 (1976).
- [6] G. Grell and S. I. Bokarev, Multi-reference protocol for (auto)ionization spectra: Application to molecules, *J. Chem. Phys.* **152**, 074108 (2020).
- [7] P. V. Demekhin, A. Ehresmann, and V. L. Sukhorukov, Single center method: A computational tool for ionization and electronic excitation studies of molecules, *J. Chem. Phys.* **134**, 024113 (2011).
- [8] H. Bachau, E. Cormier, P. Decleva, J. E. Hansen, and F. Martín, Applications of  $B$ -splines in atomic and molecular physics, *Rep. Prog. Phys.* **64**, 1815 (2001).
- [9] C. Marante, M. Klinker, I. Corral, J. González-Vázquez, L. Argenti, and F. Martín, Hybrid-Basis close-coupling interface to quantum chemistry packages for the treatment of ionization problems, *J. Chem. Theory Comput.* **13**, 499 (2017).
- [10] T. Åberg, G. Howat, L. Karlsson, J. A. R. Samson, H. Siegbahn, and A. F. Starace, *Corpuscles and Radiation in Matter I*, edited by W. Mehlhorn, Encyclopedia of Physics, Vol. 31 (Springer, Berlin, 1982).
- [11] P. G. Burke, *R-Matrix Theory of Atomic Collisions: Application to Atomic, Molecular and Optical Processes*, Springer Series on Atomic, Optical, and Plasma Physics No. 61 (Springer, Heidelberg, Germany, 2011).
- [12] H. Friedrich, *Scattering Theory*, Lecture Notes in Physics No. Vol. 872 (Springer, Heidelberg, Germany, 2013).
- [13] C. M. Oana and A. I. Krylov, Cross sections and photoelectron angular distributions in photodetachment from negative ions using equation-of-motion coupled-cluster Dyson orbitals, *J. Chem. Phys.* **131**, 124114 (2009).
- [14] F. L. Yip, C. W. McCurdy, and T. N. Rescigno, Hybrid orbital and numerical grid representation for electronic continuum processes: Double photoionization of atomic beryllium, *Phys. Rev. A* **81**, 053407 (2010).

- [15] R. Matsuzaki and S. Yabushita, Optimization of complex slater-type functions with analytic derivative methods for describing photoionization differential cross sections, *J. Comput. Chem.* **38**, 910 (2017).
- [16] R. Szmytkowski and M. Gruchowski, Ingoing and outgoing waves in the non-relativistic theory of photoionization, *J. Quant. Spectrosc. Radiat. Transfer* **94**, 127 (2005).
- [17] P. W. Langhoff, S. T. Epstein, and M. Karplus, Aspects of Time-dependent perturbation theory, *Rev. Mod. Phys.* **44**, 602 (1972).
- [18] R. V. Vedrinskiy and I. I. Geguzin, *Solid-State X-Ray Absorption Spectra [in Russian]* (Energoatomizdat, Moscow, 1991).
- [19] C. W. McCurdy, M. Baertschy, and T. N. Rescigno, Solving the three-body Coulomb breakup problem using exterior complex scaling, *J. Phys. B: At. Mol. Opt. Phys.* **37**, R137 (2004).
- [20] C. Brion and F. Carnovale, The absolute partial photoionization cross section for the production of the  $x^2b_1$  state of  $H_2O^+$ , *Chem. Phys.* **100**, 291 (1985).
- [21] K. Tan, C. Brion, P. Van der Leeuw, and M. van der Wiel, Absolute oscillator strengths (10–60 eV) for the photoabsorption, photoionisation and fragmentation of  $H_2O$ , *Chem. Phys.* **29**, 299 (1978).
- [22] C. M. Truesdale, S. Southworth, P. H. Kobrin, D. W. Lindle, G. Thornton, and D. A. Shirley, Photoelectron angular distributions of  $H_2O$ , *J. Chem. Phys.* **76**, 860 (1982).
- [23] M. S. Banna, B. H. McQuaide, R. Malutzki, and V. Schmidt, The photoelectron spectrum of water in the 30 to 140 eV photon energy range, *J. Chem. Phys.* **84**, 4739 (1986).
- [24] T. Moitra, A. Ponzi, H. Koch, S. Coriani, and P. Decleva, Accurate Description of photoionization dynamical parameters, *J. Phys. Chem. Lett.* **11**, 5330 (2020).
- [25] N. C. Handy, M. T. Marron, and H. J. Silverstone, Long-range behavior of Hartree-Fock orbitals, *Phys. Rev.* **180**, 45 (1969).
- [26] A. Sommerfeld, *Partial Differential Equations in Physics* (Elsevier Science, Burlington, MA, 2014).
- [27] P. Bettess, *Infinite Elements*, 1st ed. (Penshaw, Cleadon, England, 1992).
- [28] F. Ihlenburg, *Finite Element Analysis of Acoustic Scattering* (Springer, New York, 1998).
- [29] C. H. Wilcox, A generalization of theorems of Rellich and Atkinson, *Proc. Amer. Math. Soc.* **7**, 271 (1956).
- [30] D. Dreyer and O. Von Estorff, Improved conditioning of infinite elements for exterior acoustics, *Int. J. Numer. Methods Eng.* **58**, 933 (2003).
- [31] B. S. Kirk, J. W. Peterson, R. H. Stogner, and G. F. Carey, libMesh : A C++ library for parallel adaptive mesh refinement/coarsening simulations, *Eng. Comput.* **22**, 237 (2006).
- [32] R. J. Astley, Infinite elements for wave problems: A review of current formulations and an assessment of accuracy, *Int. J. Numer. Methods Eng.* **49**, 951 (2000).
- [33] R. J. Astley, G. J. Macaulay, J. P. Coyette, and L. Cremers, Three-dimensional wave-envelope elements of variable order for acoustic radiation and scattering. Part I. Formulation in the frequency domain, *J. Acoust. Soc. Am.* **103**, 49 (1998).
- [34] H. Si, TetGen, a Delaunay-based quality tetrahedral mesh generator, *ACM Trans. Math. Softw.* **41**, 1 (2015).
- [35] D. W. Kelly, J. P. De S. R. Gago, O. C. Zienkiewicz, and I. Babuska, A posteriori error analysis and adaptive processes in the finite element method: Part I—error analysis, *Int. J. Numer. Meth. Engng.* **19**, 1593 (1983).
- [36] M. J. Frisch, G. W. Trucks, H. B. Schlegel, G. E. Scuseria, M. A. Robb, J. R. Cheeseman, G. Scalmani, V. Barone, G. A. Petersson, H. Nakatsuji, X. Li, M. Caricato, A. V. Marenich, J. Bloino, B. G. Janesko, R. Gomperts, B. Mennucci, H. P. Hratchian, J. V. Ortiz, A. F. Izmaylov *et al.*, GAUSSIAN 16 Revision C.01 (2016), <http://gaussian.com/citation/>.
- [37] T. Van Mourik, Jr., A. K. Wilson, and T. H. Dunning, Benchmark calculations with correlated molecular wave functions. XIII. Potential energy curves for  $He_2$ ,  $Ne_2$  and  $Ar_2$  using correlation consistent basis sets through augmented sextuple zeta, *Mol. Phys.* **96**, 529 (1999).
- [38] T. Van Mourik and T. H. Dunning, Jr., Gaussian basis sets for use in correlated molecular calculations. VIII. Standard and augmented sextuple zeta correlation consistent basis sets for aluminum through argon, *Int. J. Quantum Chem.* **76**, 205 (2000).
- [39] K. A. Peterson, D. E. Woon, and T. H. Dunning, Benchmark calculations with correlated molecular wave functions. IV. The classical barrier height of the  $H + H_2 \rightarrow H_2 + H$  reaction, *J. Chem. Phys.* **100**, 7410 (1994).
- [40] A. K. Wilson, T. van Mourik, and T. H. Dunning, Gaussian basis sets for use in correlated molecular calculations. VI. Sextuple zeta correlation consistent basis sets for boron through neon, *J. Mol. Struct. (THEOCHEM)* **388**, 339 (1996).
- [41] T. Möhle, O. S. Bokareva, G. Grell, O. Kühn, and S. I. Bokarev, Tuned Range-separated density functional theory and Dyson orbital formalism for photoelectron spectra, *J. Chem. Theory Comput.* **14**, 5870 (2018).
- [42] A. F. Starace, Trends in the theory of atomic photoionization, *Appl. Opt.* **19**, 4051 (1980).
- [43] M. Ruberti, V. Averbukh, and P. Decleva, B-spline algebraic diagrammatic construction: Application to photoionization cross-sections and high-order harmonic generation, *J. Chem. Phys.* **141**, 164126 (2014).
- [44] H. J. Wörner, H. Niikura, J. B. Bertrand, P. B. Corkum, and D. M. Villeneuve, Observation of Electronic Structure Minima in High-Harmonic Generation, *Phys. Rev. Lett.* **102**, 103901 (2009).
- [45] J. Samson and W. Stolte, Precision measurements of the total photoionization cross-sections of He, Ne, Ar, Kr, and Xe, *J. Electron Spectrosc. Relat. Phenom.* **123**, 265 (2002).
- [46] R. Houlgate, J. West, K. Codling, and G. Marr, The angular distribution of the  $3p$  electrons and the partial cross section of the  $3s$  electrons of argon from threshold to 70 eV, *J. Electron Spectrosc. Relat. Phenom.* **9**, 205 (1976).
- [47] B. Möbus, B. Magel, K.-H. Scharfner, B. Langer, U. Becker, M. Wildberger, and H. Schmoranzner, Measurements of absolute Ar  $3s$  photoionization cross sections, *Phys. Rev. A* **47**, 3888 (1993).
- [48] R. G. Houlgate, K. Codling, G. V. Marr, and J. B. West, Angular distribution and photoionization cross section measurements on the  $3p$  and  $3s$  subshells of argon, *J. Phys. B* **7**, L470 (1974).
- [49] T. Marx and S. I. Bokarev (unpublished).
- [50] J. Muga, J. Palao, B. Navarro, and I. Egusquiza, Complex absorbing potentials, *Phys. Rep.* **395**, 357 (2004).
- [51] T. Carette, J. M. Dahlström, L. Argenti, and E. Lindroth, Multiconfigurational Hartree-Fock close-coupling ansatz: Application to the argon photoionization cross section and delays, *Phys. Rev. A* **87**, 023420 (2013).